Analytical potential energy surface for the CH4+Cl→CH3+ClH reaction: Application of the variational transition state theory and analysis of the kinetic isotope effects

ARTICLE *in* THE JOURNAL OF CHEMICAL PHYSICS · AUGUST 1996

Impact Factor: 2.95 · DOI: 10.1063/1.472219

2 AUTHORS:

Joaquin Espinosa-Garcia
Universidad de Extremadura
141 PUBLICATIONS **2,171** CITATIONS
SEE PROFILE

Jose C Corchado
Universidad de Extremadura
118 PUBLICATIONS **3,273** CITATIONS
SEE PROFILE

Analytical potential energy surface for the $CH_4+Cl\rightarrow CH_3+ClH$ reaction: Application of the variational transition state theory and analysis of the kinetic isotope effects

J. Espinosa-García[a] and J. C. Corchado
Departamento de Química Física, Universidad de Extremadura 06071 Badajoz, Spain

(Received 1 March 1996; accepted 24 May 1996)

We present a potential energy surface for the $CH_4+Cl\rightarrow CH_3+Cl$ reaction, based on the analytical function $J1$ for the analog $CH_4+H\rightarrow CH_3+H_2$ reaction by Joseph *et al.* To calibrate the new surface we chose the reactant and product experimental properties as reference data. The forward and reverse rate constants were calculated using variational transition state theory with large curvature transmission coefficients over a wide temperature range, 200–1000 K. The variational effects were concluded to be small for this reaction, and good agreement with experimental rate constants was found in both forward and reverse reactions. The kinetic isotope effects (KIEs) at different temperatures for the forward and reverse reactions were also analyzed showing always a ''normal'' behavior. The factor analysis of the KIEs in the forward reactions indicated high vibrational and tunneling contributions at low temperatures. © *1996 American Institute of Physics.*
[S0021-9606(96)02033-8]

I. INTRODUCTION

It is well known that the complete construction of an analytical potential energy surface (PES) of polyatomic reactions is not a trivial task and is time consuming. However, sometimes it is possible to make use of the knowledge of the PES in similar reactions and with the proper modifications to build the analytical PES for the new reaction. This strategy is less time consuming and, compared with other methods which describe a chemical reaction by using theoretical electronic structure information only in the region of configuration space along a reaction path without an intermediary potential surface fit, it has the advantage that it describes the wide reaction region of geometries accessed by tunneling paths when the reaction-path curvature is large.

In the present paper, we use this strategy to build the analytical PES for the $CH_4+Cl\rightarrow CH_3+ClH$ gas-phase reaction based on the analytical function $J2$ for $CH_4+H\rightarrow CH_3+H_2$ by Joseph *et al.*[1] In a previous paper[2] we build an analytical PES for the $CH_4+F\rightarrow CH_3+FH$ reaction using the same methodology. In that paper the strengths and the weaknesses of this strategy with respect to other methods of describing the chemical reaction were analyzed. As other methods, we used the ''direct dynamics'' method[3] which employs *ab initio* electronic structure information only in the region along the reaction path, and a low-cost semiempirical numerical surface which uses semiempirical electronic structure information in the reaction path and in the wide reaction-swath region[3(b)] of geometries accessed by tunneling paths.

The $CH_4+Cl\rightarrow CH_3+ClH$ reaction is an interesting system because it represents a heavy–light–heavy mass combination which is a good candidate for a large tunneling effect and, therefore, requires a wider description of the reaction region than that given by methods which only describe the minimum energy path (MEP). Due to its importance in atmospheric chemistry, the title reaction has been widely studied from an experimental[4–16] and theoretical[17–22] point of view. Theoretically, Truhlar *et al.*[17] and Chen *et al.*[18] using extensive *ab initio* calculations have provided geometric, vibrational and energetic information at the stationary points, but do not calculate reaction rates. Chen *et al.*[19] for the reverse reaction calculated rate constants based on RRKM theory[23] with correction for tunneling evaluated using the simple Wigner factor,[24] obtaining excellent agreement with experimental values. However, since the Wigner factor underestimates the tunneling effect, this agreement must be due to error cancelation. Gonzalez-Lafont *et al.*[20] used this reaction as test of the useful interpolation methods to calculate rate constants from electronic structure calculations. They used *ab initio* information only at five points along the reaction path, reactants, products, saddle point, plus two extra points, using their previous *ab initio* results.[17] With this information, they calculated the rate constants using canonical variational transition state theory (CVT) with multidimensional semiclassical tunneling corrections of small curvature (SCT), concluding that the interpolated calculations agree with the experimental values within a factor of 5.5 for the worst model at 300 K, which is quite reasonable for a totally *ab initio* prediction based on five points along the reaction path. Dobbs and Dixon[21] using conventional transition state theory calculated the rate constants at different temperatures. They concluded that the calculated rates are too low as compared to experiments at low temperatures, but that there is reasonable agreement for $T>300$ K. Recently, Duncan and Truong[22] have calculated the rate constants using the CVT/SCT methodology, based only on *ab initio* information on the reaction path. Their CVT/SCT rate constants are noticeably lower than the experimental values by factors increasing

[a]Author to whom correspondence should be addressed.

from 1.7 to 10 as the temperature decreases from 500 to 200 K.

II. METHODS AND CALCULATION DETAILS

A. Calibration of the analytical PES

The $CH_4+Cl\rightarrow CH_3+ClH$ reaction presents notable similarities to the well-studied $CH_4+H\rightarrow CH_3+H_2$ reaction.[1,25] Both are hydrogen abstraction reactions from methane to yield the CH_3 radical, and there is a slow change in geometry of the CH_3 group from pyramidal to planar during these reactions.

With this idea in mind, we have modified several parameters of the original surface by Joseph *et al.*[1] for the $CH_4+H\rightarrow CH_3+H_2$ reaction in order to get an analytical surface capable of representing the dynamics of the $CH_4+Cl\rightarrow CH_3+ClH$ reaction.

There are at least two methods to calibrate an analytical PES. One is to calibrate the PES to reproduce the experimental rate constants if we are interested in other features of the reaction dynamics. Another is to calibrate the PES to obtain good agreement with the reactant, product, and saddle-point properties (vibrational frequencies, and heat of reaction) if we are also interested in the rate constants. In this paper, we use this last option, which has already been used by us in previous studies on hydrogen abstraction reactions to improve the reaction path, with excellent results.[2,26,27] The saddle-point properties chosen for calibrating our surface were the barrier height, the geometry and the vibrational frequencies. Analyzing the available theoretical calculations,[17–22] the second-order Møller–Plesset perturbation theory (MP2) extrapolated to complete basis sets and full inclusion of correlation energy by ''scaling all correlation'' (SAC) method by Truhlar *et al.*[17] seems to reproduce best the experimental heat of reaction and activation energy.

Besides the stationary points along the reaction path (reactants, products and saddle point), a loosely hydrogen-bonded complex with C_{3v} symmetry near the products (CH_3...HCl) has been theoretically found,[18,22] although there is some disagreement about its stability with respect to the products: 0.67 kcal mol^{-1} (Ref. 18) using GAUSSIAN 1 theory, or 2.32 kcal mol^{-1} (Ref. 22) using a combined density functional and molecular orbital approach.

With respect to the original $J1$ surface,[1] we adjusted the various $D^{(3)}_{X-Y}$, b_k and c parameters of Eqs. (8), (14), and (15) in the original paper. The final values of these parameters for the new surface are: $D^{(3)}_{C-H}=0.0680$ a.u. (1.850 eV), $D^{(3)}_{Cl-H}=0.0632$ a.u. (1.720 eV), $D^{(3)}_{C-Cl}=0.0353$ a.u. (0.960 eV); $b_k=1.0\ a_0^{-1}$, and $c=0.6\ a_0^{-1}$. The R^e_{X-Y} parameters used are: C–H=2.067 a_0, Cl–H=2.409 a_0, C–Cl=3.366 a_0 (Ref. 28). The singlet potential is expressed by a Morse function with $D^{(1)}_{X-Y}=4.863$, 4.613, and 3.779 eV for C–H, Cl–H, and C–Cl, respectively.[26] Finally, the range parameters for the singlet and triplet functions, α and β, were 0.990 and 0.860 for Cl–H and C–Cl, respectively, the C–H value being calculated as described by Eq. (15) in Ref. 1. The β_{C-Cl} parameter was also varied to fit the imaginary frequency at the saddle point.

B. Computational details

With the new surface calibrated as described in the previous section, we analyzed several features of the $CH_4+Cl\rightarrow CH_3+ClH$ reaction. We calculated the rate constants using the canonical variational transition state theory (CVT), which locates the dividing surface between reactants and products along the reaction coordinate s to minimize the generalized TST rate constants, $K^{GT}(T,s)$. The reaction coordinate, s, is defined as the signed distance from the saddle point, with $s>0$ referring to the product side. The reaction path is calculated using the Page–McIver method.[29] Different step sizes were tried until variational rate constants converged. This gave us a step size of 0.05 bohr $amu^{1/2}$. In the rest of the paper, the units of s are bohr, and the reduced mass is $\mu=1$ amu. Thus, distances through the mass-scaled coordinates in bohr are equivalent to distances through mass-weighted coordinates in bohr $amu^{1/2}$. Along this minimum energy path (MEP) a generalized normal-mode analysis projecting out frequencies at each point along the path was performed.[30] With this information, we could calculate both the vibrational partition function along the MEP and the ground-state vibrationally adiabatic potential curve

$$V_a^G(s)=V_{MEP}(s)+\epsilon^G_{int}(s),$$

where $V_{MEP}(s)$ is the classical energy along the MEP with its zero energy at the reactants ($s=-\infty$), and $\epsilon^G_{int}(s)$ is the zero-point energy at s from the generalized normal-mode vibrations orthogonal to the reaction coordinate.

In the present work, we used the general polyatomic rate constant code POLYRATE.[31] The rotational partition functions were calculated classically. Also, we included correctly the $^2P_{1/2}$ excited state of Cl in the reactant electronic partition function (882 cm^{-1}).[28] Finally, we considered the tunneling corrections. This reaction presents a heavy–light–heavy mass combination and, therefore, a large-curvature tunneling (LCT) calculation is necessary. We used the LCG3 approximation[32] allowing the system to reach all the accessible vibrational excited states, since reactant and product bound modes excitation is seen to be very important in this reaction.

III. RESULTS AND DISCUSSION

A. Calibration test at the stationary points

To test the calibration for the new surface, we use the stationary point properties (reactants, products, and saddle point). The geometries of reactants and products are in excellent agreement with the experimental values.[28] With respect to the saddle point, our geometry is in accordance with other theoretical values[17,18,21] with differences smaller than 5%, although the bonds which are formed and broken are most symmetrical and the angle HC–H′ is slightly larger (107° against 101°). The vibration frequencies at the stationary points are listed in Table I. The new surface reproduces the methane, methyl, and hydrogen cloride experimental frequencies accurately and predicts also that methyl is planar and methane is tetrahedral. The other values in the literature

TABLE I. Vibrational frequencies (cm^{-1}).

	Symmetry	This work	MP-SAC2[a]	MP2[b]	BH&HLYP[c]	Expt.[d]
ClH		2994	3048	3063	3059	2889
CH_3	a_1'	2984	3176	3178	3187	3002
	a_2''	580	426	460	500	580
	e'	3172	3369	3369	3370	3184
	e'	1383	1452	1441	1453	1383
CH_4	a_1	2874	3080	3076	3107	2917
	e	1505	1582	1591	1609	1534
	t_2	3038	3217	3212	3217	3019
	t_2	1344	1364	1369	1389	1306
Complex	v_1 a_1	2942		3209	3180	
	v_2	2924		2930	2887	
	v_3	610		630	658	
	v_4	60		100	97	
	v_5 e	3086		3397	3364	
	v_5	1347		1481	1455	
	v_7	126		328	359	
	v_8	80		142	160	
Saddle point	v_1 a_1	2960	3118	3132	3162	
	v_2	1190	1227	1213	1211	
	v_3	543	572	511	541	
	v_4 e	3022	3295	3305	3328	
	v_5	1419	1441	1448	1468	
	v_6	1102	874	958	920	
	v_7	344	324	378	385	
	v_8 a_1	1196i	949i	1262i	996i	

[a]Values are taken from Ref. 17.
[b]Taken from Refs. 18 and 21.
[c]Taken from Ref. 22.
[d]Taken from Ref. 28.

overestimate the frequencies by about 5–10%. Thus, as we have calibrated our surface with respect to the fundamental frequencies, no anharmonic corrections are taken into account in the rest of paper.

The linear saddle point was identified with one negative eigenvalue of the Hessian matrix and, therefore, one imaginary frequency, intermediate between the other theoretical values.

B. Reaction path and frequency analysis

As stated above, the reaction path was calculated using the Page and McIver method,[29] with a step size of 0.05 bohr amu$^{1/2}$ which gave converged reaction paths. Figure 1 shows the minimum energy path, V_{MEP}, the ground-state vibrationally adiabatic potential energy curve, V_a^G, and its zero-point energies, as a function of s. The barrier height is 8.09 kcal mol^{-1} and the heat of reaction at 0 K is 0.97 kcal mol^{-1}, at only 0.2 kcal mol^{-1} from the experimental value.[28] The position of the maximum on the V_a^G curve appears slightly shifted with respect to the saddle point ($s=0$), $s=-0.05$ bohr, and it presents a well at $s=-0.45$ bohr. Moreover, the zero-point energy falls sharply at about the same s (-0.45 bohr) after which it declines smoothly with s. This behavior is different from that found for similar hydrogen abstraction reactions, NH_3+H,[26] NH_3+OH,[27] or CH_4+F.[2] To analyze this behavior in greater detail, in Fig. 2 we show the variation of the generalized normal mode frequencies along the reaction path.

In the negative limit of s ($s=-\infty$) there are nine frequencies corresponding to the CH_4+Cl reactants. The CH_4 symmetric stretching, corresponding to the normal mode breaking during the reaction (*reactive mode*), and the umbrella bending (t_2 symmetry) modes, drop sharply at about $s=-0.5$ bohr. The two lowest frequencies as s is varied

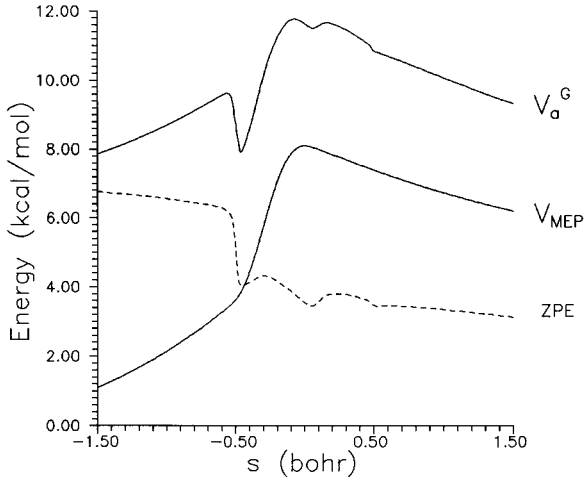

FIG. 1. Classical potential energy curve, V_{MEP}, zero-point energies, ZPE, and vibrationally adiabatic potential energy curve, V_a^G as a function of s for the unsubstitud reaction. The ZPE and the V_a^G curves are uniformly lowered by 20 kcal mol^{-1}.

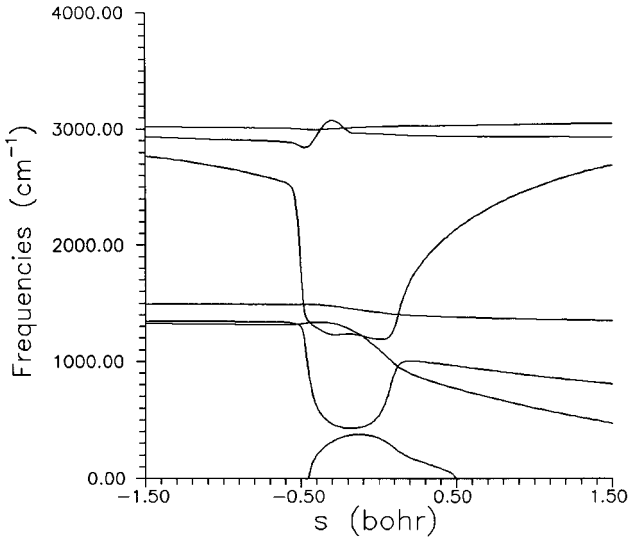

FIG. 2. Generalized normal-mode vibrational frequencies as a function of s.

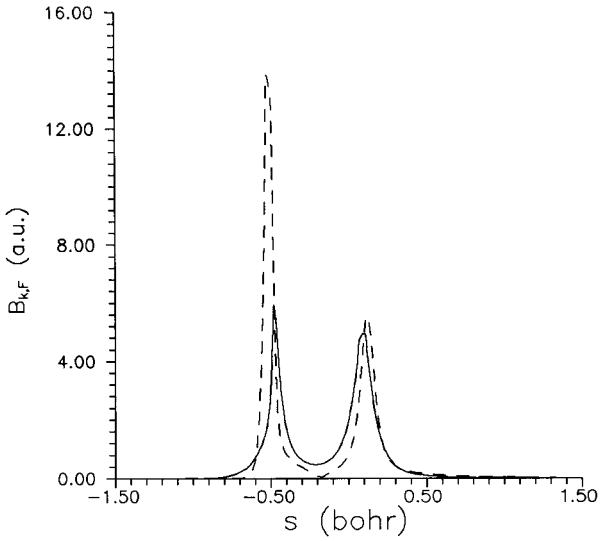

FIG. 3. Curvature elements, $B_{k,F}(s)$. Coupling along the MEP between the reaction coordinate (F) and two other bound modes.

correspond to free rotations and translations that evolve to vibrations (*transitional modes*). These transitional modes present a maximum coinciding with the minimum of the reactive and bending modes near the saddle point, although not enough to compensate them. As a result, the ZPE shows noticeable changes with s (Fig. 1) and, therefore, variational effects may be expected for this reaction. Two other factors point in this same direction. First, this reaction presents a heavy–light–heavy mass combination, which is a good candidate for large variational effects[32] (a ''variational effect'' is the difference between variational CVT and conventional TST rate constants), and second, this reaction presents only two transitional modes to compensate the decline of the reactive mode. In this sense, this reaction is more similar to an atom–diatom reaction than to a polyatomic one. However, at 0 K, the variational effect found is small, $s^*=-0.07$ bohr, due probably to the large barrier height in this reaction (8.09 kcal mol^{-1}). Thus, the energetic factor, which locates the saddle point at $s=0$, dominates over the ZPE.

The coupling between the reaction coordinate and the orthogonal bound modes, whose measure is given by the elements $B_{kF}(s)$ along the MEP, govern the nonadiabatic flow of energy between these modes and the reaction coordinate.[33] Figure 3 shows the two B_{kF} coupling terms that change most significantly as a function of s. The large B_{kF} couplings for the CH_4 symmetric stretch (dashed line) and the umbrella bend (solid line) modes indicate that excitation of these modes would greatly enhance the reaction rates. Moreover, with respect to the products, the Cl–H stretching and the CH_3 bending modes strongly couple with the reaction coordinate in the exit channel, with the B_{kF}'s attaining large values after the saddle point and, therefore, the excitation of these bonds can be expected. This result contrasts with the experimental result of Simpson *et al.*[15] who only found Cl–H vibrational excitation, and with the theoretical results found by us[2] for a similar reaction, $CH_4+F\rightarrow CH_3+FH$, where the CH_3 product is not vibrationally excited. Finally, this analysis of the reaction

TABLE II. Forward rate constants[a] for the $CH_4+Cl\rightarrow CH_3+ClH$ reaction.

T (K)	TST	CVT	CVT/SCT	CVT/LCT	Expt.[b]
200.0	0.00020	0.00015	0.00114	0.0154	0.0111
250.0	0.00197	0.00149	0.00596	0.0417	0.0434
298.0	0.00886	0.00700	0.0192	0.0857	0.0991
300.0	0.00935	0.00740	0.0200	0.0880	0.101
350.0	0.0297	0.0242	0.0511	0.162	0.214
400.0	0.0733	0.0608	0.109	0.272	0.375
450.0	0.152	0.128	0.205	0.428	0.581
500.0	0.281	0.239	0.350	0.641	0.825
600.0	0.743	0.641	0.838	1.28	
800.0	2.89	2.52	2.93	3.7	
1000.0	7.36	6.42	7.05	8.22	

[a]In 10^{-12} cm^3 molecule^{-1} s^{-1}.
[b]Taken from Arrhenius fits to experimental data (Ref. 14).

TABLE III. Reverse rate constants[a] for the $CH_4+Cl\rightarrow CH_3+ClH$ reaction.

T (K)	TST	CVT	CVT/SCT	CVT/LCT	Expt.[b]
200.0	0.00309	0.00221	0.0172	0.234	
250.0	0.0144	0.0109	0.0437	0.305	
298.0	0.0390	0.0308	0.0844	0.377	
300.0	0.0404	0.0319	0.0865	0.380	0.478
350.0	0.0854	0.0695	0.147	0.465	0.668
400.0	0.152	0.126	0.226	0.564	0.859
450.0	0.242	0.204	0.321	0.680	1.04
500.0	0.356	0.303	0.444	0.814	1.22
600.0	0.664	0.573	0.749	1.14	
800.0	1.64	1.43	1.66	2.11	
1000.0	3.19	2.78	3.05	3.56	

[a]In 10^{-13} cm^3 $molecule^{-1}$ s^{-1}.
[b]From Ref. 13.

coordinate-bound modes coupling shows that the reaction path curvature must therefore be taken into account in order to correctly calculate the tunneling effect.

C. Rate constants for the isotopically unsubstituted reaction

In the variational transition state theory the dividing surface is varied along the reaction path to minimize the rate constants. We thus obtain the generalized transition state (GTS) at the value s^*.[32] Thermodynamically, the minimum rate constant criterion is equivalent to maximizing the generalized standard-state free energy of activation, $\Delta G°(T,s)$. Therefore, the effects of the potential energy, entropy and temperature on the location of this GTS must be considered. The bottleneck properties of the reaction, based on the canonical approach (CVT), indicate that the variational effects are small, as we had anticipated in the analysis of the vibrational frequencies. The value of s ranges between -0.07 bohr at 0 K and -0.09 bohr at 1000 K. For this reaction, the energy contribution (barrier height=8.09 kcal mol^{-1}) dominates over the entropy contribution, even at high temperatures.

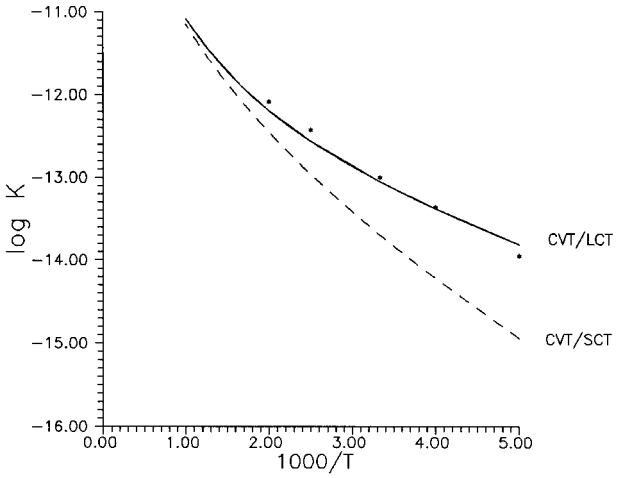

FIG. 4. Arrhenius plot of $\log_{10}$ K (cm^3 $molecule^{-1}$ s^{-1}) against the reciprocal temperature (K) in the range 200–1000 K. Dashed line is our CVT/SCT calculated forward reaction rate constant; solid line is our CVT/LCT calculation; and asterisks are the experimental values.

Tables II and III list the conventional TST, the variational CVT and the experimental rate constants for the temperature range 200–1000 K for the forward and reverse reactions, respectively. The small differences between TST and CVT rates confirms our conclusion about the small variational effects, therefore, the recrossing effects have a small effect on the reaction dynamics. With respect to the tunneling correction, as this reaction presents a heavy–light–heavy mass combination, the small-curvature (SCT) tunneling approximation underestimates the forward rate constants by factors increasing from 2.3 to 9.7 as the temperature decreases from 500 to 200 K, and the reverse rate constants by factors increasing from 2.7 to 5.5 as the temperature decreases from 500 to 300 K. When the large-curvature (LCT) tunneling is considered, good agreement with the experimental values is found in both cases. Figures 4 and 5 show these results for the experimentally measured temperature range for the forward and reverse reactions, respectively.

The excellent agreement with experimental values found by Chen *et al.*[18] for the reverse reaction, using RRKM theory with corrections for tunneling evaluated using the simple Wigner factor, is probably due to error compensation, as it is well known that the Wigner factor strongly underestimates the tunneling effect. Although the calculations of Gonzalez-Lafont *et al.*[20] and our calibration process are based on the same ab initio result at the saddle point of Truhlar *et al.*,[17] different rate constants are obtained. This is due to the fact that we calibrate our analytical PES to obtain good agreement with experimental vibrational frequencies. However, Gonzalez-Lafont *et al.* used theoretical vibrational frequencies without scaling, and it is well known that these theoretical values are overestimated. Thus, the adiabatic barrier heights are 4.4 and 3.5 kcal mol^{-1} for the forward and reverse reactions, respectively, against 3.5 and 2.3 kcal mol^{-1}, respectively, obtained by Gonzalez-Lafont *et al.* With respect to the tunneling contribution the large-curvature effect is very important, and disagrees with the hypothesis of Gonzalez-Lafont *et al.* for tunneling probabilities in asym-

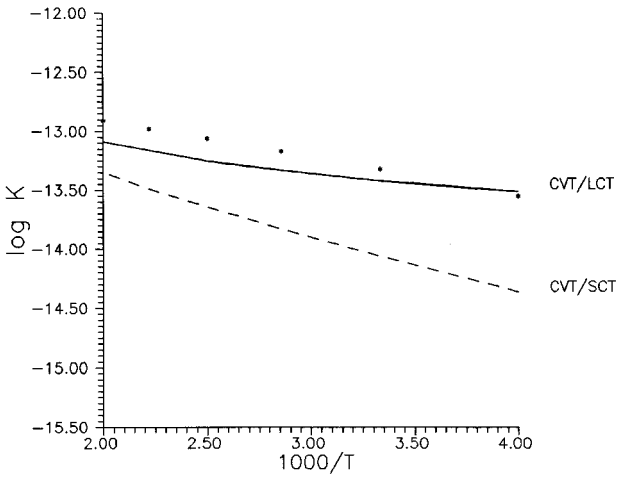

FIG. 5. As Fig. 4, but for the reverse reaction and in the range 250–500 K.

metric reactions. Thus, the differences in SCT and LCT tunneling are factors of 14., 4.4 and 2.5 at 200, 300 and 400 K, respectively.

D. Kinetic isotope effects

For the forward reaction, the calculated kinetic isotope effects (KIEs) at different temperatures with the LCT tunneling approximation are listed in Table IV for the unsubstituted and all substituted reactions:

$$CH_4+Cl\rightarrow CH_3+ClH, \quad (R1)$$

$$CD_4+Cl\rightarrow CD_3+ClD. \quad (R2)$$

To analyze their behavior in more detail, in the same Table IV we also list the factor analysis. The KIEs factorize as[34]

$$KIE=K_H/K_D=\eta_{trans}\eta_{rot}\eta_{vib}\eta_{tun}\eta_{var},$$

where η_{trans} is the ratio of the relative translational partition functions, η_{rot} is from rotation, η_{vib} is from vibration, η_{tun} is the ratio between tunneling factors $k^{LCG3}(H)/k^{LCG3}(D)$, and $\eta_{var}=KIE^{CVT}/KIE^{TST}$, i.e., the ratio of KIEs calculated using variational and conventional transition state theories. Note that the KIEs are defined as the ratio of the rate constants of (R1) to (R2). This follows the conventional approach in which the rate for the lighter isotope is always in the numerator. With this convention, KIEs greater than one are called ''normal'' and those less than one are called ''inverse.'' To the best of our knowledge, no experimentally determinated isotope data are available. All the KIEs are ''normal,'' i.e., greater than one, and they are especially large at lower temperatures. Such high normal KIEs at low temperatures result from a combination of the high vibrational and tunneling contributions. The variational contribution is close to unity, and the translational and rotational contributions are normal and independent of temperature.

For the reverse reactions

$$CH_3+ClH\rightarrow CH_4+Cl, \quad (R1)$$

$$CD_3+ClD\rightarrow CD_4+Cl, \quad (R2)$$

$$CD_3+ClH\rightarrow CD_3H+Cl, \quad (R3)$$

$$CH_3+ClD\rightarrow CH_3D+Cl, \quad (R4)$$

TABLE IV. Kinetic isotope effects[a] and factor analysis of K_1/K_2.[b]

T (K)	K_1/K_2	η_{vib}	η_{tun}	η_{var}
200.0	267.84	13.07	11.28	0.86
250.0	92.64	6.97	7.15	0.88
298.0	42.69	4.56	4.87	0.91
300.0	41.79	4.51	4.82	0.91
350.0	22.35	3.25	3.50	0.93
400.0	13.87	2.53	2.76	0.94
450.0	9.56	2.08	2.29	0.95
500.0	7.19	1.79	1.98	0.96
600.0	4.74	1.42	1.63	0.97
800.0	2.92	1.06	1.32	0.99
1000.0	2.30	0.91	1.20	1.00

[a]Calculated using CVT/LCG3 forward rate constants.
[b]η_{trans} and η_{rot} are independent of temperature, and their values are 1.25 and 1.69, respectively.

TABLE V. Kinetic isotope effects for the reverse reactions.

	CD_3+ClD		CD_3+ClH		CH_3+ClD	
T (K)	TST/W[a]	CVT/LCT[b]	TST/W	CVT/LCT	TST/W	CVT/LCT
200.0	3.70	19.68	0.37	1.90	10.47	29.52
250.0	3.48	12.57	0.49	1.89	7.23	18.04
298.0	3.25	8.75	0.59	1.81	5.57	11.87
300.0	3.23	8.64	0.59	1.80	5.52	11.68
350.0	3.01	6.42	0.67	1.68	4.49	8.20
400.0	2.80	5.10	0.74	1.57	3.81	6.20
450.0	2.63	4.24	0.79	1.48	3.34	4.96
500.0	2.47	3.66	0.83	1.40	2.99	4.15
600.0	2.23	2.94	0.88	1.30	2.52	3.20
800.0	1.92	2.26	0.94	1.18	2.04	2.36
1000.0	1.74	1.95	0.97	1.12	1.80	2.00

[a]Calculated using CVT/LCG3 reverse rate constants.
[b]Calculated using TST/Wigner reverse rate constants.

the calculated KIEs at different temperatures with LCT tunneling approximation are listed in Table V. As before, all the KIEs are ''normal'' and both (R2) and (R4) show significant kinetic isotope effects at lower temperatures. These results agree with the theoretical values of Chen *et al.*,[19] who use RRKM theory with the Wigner factor, except for K_1/K_3, where they found ''inverse'' KIEs (0.62) at 296 K. When we used this same simple Wigner factor (see Table V), we found the same result. We therefore think that this erroneous ''inverse'' value is due to the relative failure of the Wigner factor to correctly describe the tunneling correction, as is well known.

IV. CONCLUSIONS

In this work, we have obtained the potential energy surface for the $CH_4+Cl\rightarrow CH_3+ClH$ reaction based on the analytical function $J1$ for the $CH_4+H\rightarrow CH_3+H_2$ reaction, using as calibration criterion the reactant and product experimental properties, i.e., vibrational frequencies and heat of reaction, and *ab initio* saddle point and complex properties. The forward and reverse rate constants were calculated for the temperature range 200–1000 K using canonical variational transition state theory, and as this reaction presents a heavy–light–heavy mass combination, a large-curvature tunneling calculation was used. In spite of this mass combination, we found that the variational effects are small for this reaction and, therefore, the recrossing effects have a small effect on the reaction dynamics.

The kinetic isotope effects (KIEs) at different temperatures for the forward and reverse reactions were also analyzed to determine the importance of other surface features. All KIEs show a ''normal'' behavior, i.e., that the ratio of the unsubstituted/substituted rate constants is greater than one. Finally, the factor analysis of the KIEs in the forward reaction indicates high vibrational and tunneling contributions at low temperatures. Unfortunately, no experimentally determined isotope data are available, and any future experimental studies of these KIEs would be invaluable in assessing the quality of the new surface.

ACKNOWLEDGMENTS

The authors would like to thank the Dirección General de Investigación Científica y Técnica del Ministerio de Educación y Ciencia (Spain) for partial support of this work (Project No. PB94-1030), and one of us (J.C.C.) thanks Junta de Extremadura (Spain) for a scholarship.

[1] T. Joseph, R. Steckler, and D. G. Truhlar, J. Chem. Phys. **87**, 7036 (1987).
[2] J. C. Corchado and J. Espinosa-García, J. Chem. Phys. **105**, 3160 (1996).
[3] (a) K. M. Baldridge, M. S. Gordon, R. Steckler, and D. G. Truhlar, J. Phys. Chem. **93**, 5107 (1989); (b) D. G. Truhlar and M. S. Gordon, Science, **249**, 491 (1990).
[4] F. S. Rowland and M. J. Molina, Rev. Geophys. Space Phys., **13**, 1 (1975).
[5] D. A. Whytock, J. Chem. Phys. **66**, 1690 (1977).
[6] M. S. Zahniser, B. M. Berquist, and F. Kaufman, Int. J. Chem. Kin. **10**, 15 (1978).
[7] M. H. Beghal-Vayjooee, J. Am. Chem. Soc. **100**, 3214 (1978).
[8] L. F. Keyser, J. Chem. Phys. **69**, 214 (1978).
[9] C. L. Lin, M. T. Len, and W. B. DeMore, J. Phys. Chem. **82**, 1772 (1978).
[10] A. R. Ravishankara and P. H. Wine, J. Chem. Phys. **72**, 25 (1980).
[11] S. P. Heneghan, P. A. Knoot, and S. W. Benson, Int. J. Chem. Kin. **13**, 677 (1981).
[12] O. Dobis and S. W. Benson, Int. J. Chem. Kin. **19**, 691 (1987).
[13] J. J. Russel, J. A. Setula, and D. Gutman, Int. J. Chem. Kin. **20**, 759 (1988).
[14] W. B. DeMore, S. P. Sander, D. M. Golden, R. F. Hampson, M. J. Kurylo, C. J. Howard, A. R. Ravishankara, C. E. Kolb, and M. J. Molina, in JPL publication 92-20 (Jet Propulsion Laboratory, Pasadena, CA, 1992).
[15] W. R. Simpson, A. J. Orr-Ewing, and R. N. Zare, Chem. Phys. Lett. **212**, 1963 (1993).
[16] J. V. Seely, T. J. Jayne, and M. J. Molina, J. Phys. Chem. **100**, 4019 (1996).
[17] T. N. Truong, D. G. Truhlar, K. K. Baldridge, M. S. Gordon, and R. Steckler, J. Chem. Phys. **90**, 7137 (1989).
[18] Y. Chen, E. Tschuikow-Roux, and A. Rauk, J. Phys. Chem. **95**, 9832 (1991).
[19] Y. Chen, A. Rauk, and E. Tschuikow-Roux, J. Phys. Chem. **95**, 9900 (1991).
[20] A. Gonzalez-Lafont, T. N. Truong, and D. G. Truhlar, J. Chem. Phys. **95**, 8875 (1991).
[21] K. D. Dobbs and D. A. Dixon, J. Phys. Chem. **98**, 12584 (1994).
[22] W. T. Duncan and T. N. Truong, J. Chem. Phys. **103**, 9642 (1995).
[23] P. J. Robinson and K. A. Holbrook, *Unimolecular Reactions* (Wiley, New York, 1972).
[24] E. P. Wigner, Z. Phys. Chem. Abt. B **19**, 203 (1932).
[25] R. Steckler, K. J. Dykema, F. B. Brown, G. C. Hancock, D. G. Truhlar, and T. Valencich, J. Chem. Phys. **87**, 7024 (1987).
[26] J. Espinosa-García and J. C. Corchado, J. Chem. Phys. **101**, 1333 (1994).
[27] J. Espinosa-García and J. C. Corchado, J. Chem. Phys. **101**, 8700 (1994).
[28] *JANAF Thermochemical Tables*, edited by M. W. Chase Jr., C. A. Davies, J. R. Downey, D. J. Frurip, R. A. McDonald, A. N. Syverud (National Bureau of Standards, Washington D. C., 1985), Vol. 14, 3rd ed.
[29] M. Page and J. W. McIver, J. Chem. Phys. **88**, 922 (1988).
[30] W. H. Miller, N. C. Handy, and J. E. Adams. J. Chem. Phys. **72**, 99 (1980).
[31] R. Steckler, W.-P. Hu, Y.-P. Liu, G. C. Lynch, B. C. Garrett, A. D. Isaacson, D.-h. Lu, V. S. Melissas, T. N. Truong, S. N. Rai, G. C. Hancock, J. G. Lauderdale, T. Joseph, and D. G. Truhlar, *POLYRATE* (University of Minnesota, Minneapolis, 1994), Version 6.2.
[32] D. G. Truhlar, A. D. Isaacson, and B. C. Garrett, in *The Theory of Chemical Reactions*, edited by M. Bear (Chemical Rubber, Boca Raton, FL, 1985), Vol. 4.
[33] E. Kraka and T. H. Dunning, Jr., in *Advances in Molecular Electronic Structure Theory* (JAI, 1990), Vol. I, pp. 129–173.
[34] (a) A. González-Lafont, T. N. Truong, and D. G. Truhlar, J. Phys. Chem. **95**, 4618 (1991); (b) B. C. Garrett, D. G. Truhlar, and A. W. Magnuson, J. Chem. Phys. **76**, 2321 (1982); (c) S. C. Tucker, D. G. Truhlar, B. C. Garrett, and A. D. Isaacson, *ibid*. **82**, 4102 (1985); (d) D.-h. Lu, D. Maurice, D. G. Truhlar, J. Am. Chem. Soc. **112**, 6206 (1990); (e) X. G. Zhao, S. C. Tucker, and D. G. Truhlar, *ibid*. **113**, 826 (1991); (f) X. G. Zhao, D.-h. Lu, Y.-P. Liu, G. C. Lynch, and D. G. Truhlar, J. Chem. Phys. **97**, 6369 (1992); (g) D. G. Truhlar, D.-h. Lu, S. C. Tucker, X. G. Zhao, A. González-Lafont, T. N. Truong, D. Maurice, Y.-P. Liu, and G. C. Lynch. ACS Symp. Ser., No. 502, 16 (1992); (h) W.-P. Hu and D. G. Truhlar, J. Am. Chem. Soc. **116**, 7797 (1994).